Chapter VIII

Study of Slip Flow Mixed Convection Chemically Reacting Fluid past a Semi-infinite Vertical Porous Plate with Heat Source

Some part of this chapter has been accepted for publication in the UGC approved Journal entitled- Far East Journal of Applied Mathematics.

8.1 Introduction:

The study of Magnetohydrodynamic free convection finds applications in fluid engineering problems such as MHD pumps, accelerators and flow meters, plasma studies, nuclear reactors, geothermal energy extraction, *etc.* Free convective flow past a vertical plate in the presence of a transverse magnetic field has been studied by several researchers. Kim (2000) studied the magnetohydrodynamic convective heat transfer past a semi-infinite vertical porous moving plate with variable suction. The combined effects of thermal and mass diffusion on the unsteady free convection flow of a viscous incompressible fluid over an infinite vertical porous plate was investigated by Takhar *et al.* (2003). Ahmed *et al.* (2011) considered the effects of thermal diffusion on a three-dimensional MHD free convection flow of a viscous incompressible fluid over a vertical plate embedded in a porous medium. Choudhury and Hazarika (2013) examined the effects of variable viscosity and thermal conductivity on free convective oscillatory flow of a viscous incompressible and electrically conducting fluid past a vertical plate in slip flow regime with periodic plate temperature when suction velocity oscillates in time about a constant mean.

The combined effects of convective heat and mass transfer on the flow of a viscous, incompressible and electrically conducting fluid has many engineering and geophysical applications such as in geothermal reservoirs, drying of porous solids, thermal insulation, enhanced oil recovery, cooling of nuclear reactor and underground energy transports. The hydromagnetic free convection flow with mass transfer effect has been studied extensively by many researchers. Chamkha and Khaled (2000) investigated the hydromagnetic combined heat and mass transfer by natural convection from a permeable surface embedded in a fluid saturated porous medium. Chen (2004) studied the combined heat and mass transfer in MHD free convection from a vertical surface with Ohmic heating and viscous dissipation. Lai and Kulachi (1990) used the series expansion method to investigate coupled heat and mass transfer in natural convection from a sphere in a porous medium. The heat and mass transfer effects on a flow along a vertical plate in the presence of magnetic field was

investigated by Elbashbeshy (1997). The influence of combined natural convection from a vertical wavy surface due to thermal and mass discussion was studied by Hossain and Rees (1999).

Heat absorption/generation effects have significant impact on the heat and mass transfer flow of a viscous, incompressible and electrically conducting fluid. Chamkha and Khaled (2001) investigated heat generation/absorption effects on hydromagnetic combined heat and mass transfer flow from an inclined plate. The effects of a heat source/sink on unsteady MHD convection through porous medium with combined heat and mass transfer was studied by Kamel (2001). Chamkha (2004) solved the problem of unsteady MHD convective heat and mass transfer past a semi-infinite vertical permeable moving plate with heat absorption. Makinde (2009) discussed the hydromagnetic boundary layer flow and mass transfer past a vertical plate in a porous medium with constant heat flux.

There has been a renewed interest in studying magnetohydrodynamic flow with heat and mass transfer in porous and nonporous media in the presence of magnetic field due to its importance in the design of MHD generators and accelerators in geo-physics, in systems like underground water and energy storage, The effect of transversely applied magnetic field on convection flows of an electrically conducting fluid has been discussed by several authors notably Nigam and Singh (1960), Soundalgekar and Bhat (1971), Vajravelu (1988), Attia and Kotb (1996) etc. The effect of chemical reaction on above discussed flow is very useful for improving a number of chemical technologies such as food processing, polymer production, manufacturing of ceramics etc. Chamber and Young (1958) analyzed the effects of homogeneous first order chemical reactions in the neighbourhood of a plate for destructive and generative reactions. Muthucumaraswamy *et al.* (2008) studied the mass transfer effect on isothermal vertical oscillating plate in presence of chemical reaction. Ahmed (2014) numerically analyzed the magneto hydrodynamic chemically reacting and radiating fluid past a non-isothermal impulsively started vertical surface adjacent to a porous regime.

On the other hand radiative flows are encountered in countless industrial and environmental processes e.g. heating and cooling chambers, fossil fuel combustion and energy processes evaporation from large open water reservoirs and solar power technology. Soundalgekar and Takhar (1993) considered the radiative free convective flow of an optically thin gray-gas past a semi-infinite vertical plate. Raptis and perdikis (1999) studied the effects of thermal radiation and free convection flow past a moving vertical plate. Kartikeyan *et al.* (2013) investigated the thermal radiation effects on MHD convective flow over a plate in a porous medium by perturbation technique. Ahmed *et al.* (2014) approached Non-linear Magneto hydrodynamic radiating flow over an impulsively started vertical plate in a saturated porous regime with Laplace and Numerical technique.

The aim of this chapter is to investigate effects of chemical reaction and mass transfer in a slip flow for MHD convective flow of an unsteady viscous incompressible electrically conducting fluid over a semi-infinite vertical plate embedded in a porous medium with heat generation effect. The validity of the flow model has been discussed fruitfully. The non-linear partial differential equations have been solved analytically using classical perturbation technique.

8.2 Mathematical formulation:

The laminar convective heat and mass transfer flow of an incompressible, viscous, heat absorbing, electrically conducting fluid over a semi-infinite vertical plate with radiation embedded in a porous medium is considered. A uniform magnetic field of strength B_0 is applied transversely in the direction of $\bar{y}$ axis. The $\bar{x}$ axis is taken along the plate and $\bar{y}$ is perpendicular to it. The induced magnetic field is neglected. The radiative heat flux in the $\bar{x}$ direction is considered negligible in comparison to that in the $\bar{y}$ direction. Then by usual Boussinesq's approximation the unsteady flow is governed by the following equations

$$\frac{\partial \bar{u}}{\partial \bar{t}} + \bar{v}\frac{\partial \bar{u}}{\partial \bar{y}} = \begin{cases} -\dfrac{1}{\rho}\dfrac{\partial \bar{p}}{\partial \bar{x}} + v\dfrac{\partial^2 \bar{u}}{\partial \bar{y}^2} + g\beta(\bar{T} - \bar{T}_\infty) \\[2mm] +g\bar{\beta}(\bar{C} - \bar{C}_\infty) - \left(\dfrac{\sigma B_0^2}{\rho} + \dfrac{v}{K}\right)\bar{u} \end{cases}, \tag{8.2.1}$$

$$\frac{\partial \bar{T}}{\partial \bar{t}} + \bar{v}\frac{\partial \bar{T}}{\partial \bar{y}} = \frac{\kappa}{\rho C_p}\frac{\partial^2 \bar{T}}{\partial \bar{y}^2} - \frac{1}{\rho C_p}\left(\frac{\partial \bar{q}_r}{\partial \bar{y}}\right) - \frac{Q_0}{\rho C_p}(\bar{T} - \bar{T}_\infty), \tag{8.2.2}$$

$$\frac{\partial \bar{C}}{\partial \bar{t}} + \bar{v}\frac{\partial \bar{C}}{\partial \bar{y}} = D\frac{\partial^2 \bar{C}}{\partial \bar{y}^2} - \bar{C}_r(\bar{C} - \bar{C}_\infty), \tag{8.2.3}$$

According to Cogley *et al.* (1968), in the optical thin limit for a non-gray gas near equilibrium, the radiative heat flux is represented by the following form

$$\frac{\partial \bar{q}_r}{\partial \bar{y}} = 4(\bar{T} - \bar{T}_\infty)\bar{I}, \tag{8.2.4}$$

where $\bar{I} = \displaystyle\int K_{\lambda w}\frac{\partial e_{b\lambda}}{\partial \bar{T}}\,d\lambda$

Under the above assumption, the boundary conditions are

$$\begin{cases} \bar{u} = \bar{u}_{slip} = \dfrac{\sqrt{K}}{\alpha}\dfrac{\partial \bar{u}}{\partial \bar{y}}, \quad \bar{T} = \bar{T}_w, \quad \bar{C} = \bar{C}_w, \quad at\ \bar{y} = 0 \\[3mm] \bar{u} \to \bar{U}_\infty = U_0(1 + \varepsilon e^{\bar{n}\bar{t}}), \quad \bar{T} \to \bar{T}_\infty, \quad \bar{C} \to \bar{C}_\infty\ as\ \bar{y} \to \infty \end{cases} \tag{8.2.5}$$

Since the suction velocity normal to the plate is a function of time only, it can be taken in the experimental form as

$$\bar{v} = -V_0(1 + \varepsilon e^{\bar{n}\bar{t}}), \tag{8.2.6}$$

where A is a real positive constant, ε and εA are small less than unity and v_0 is a scale of suction velocity which has non-zero positive constant.

Outside the boundary layer, the equation (8.2.1) becomes

$$-\frac{1}{\rho}\frac{\partial \bar{p}}{\partial \bar{x}} = \frac{d\bar{U}_\infty}{d\bar{t}} + \frac{\sigma B_0^2}{\rho}\bar{U}_\infty + \frac{\nu}{\bar{K}}\bar{U}_\infty \tag{8.2.7}$$

Eliminating $(\partial \bar{p}/\partial \bar{x})$ from equation (8.2.1) and equation (8.2.7), we obtain

$$\frac{\partial \bar{u}}{\partial \bar{t}} + \bar{v}\frac{\partial \bar{u}}{\partial \bar{y}} = \left\{ \begin{array}{l} \dfrac{d\bar{U}_\infty}{d\bar{t}} + \nu\dfrac{\partial^2 \bar{u}}{\partial \bar{y}^2} + g\beta(\bar{T} - \bar{T}_\infty) \\[4mm] + g\bar{\beta}(\bar{C} - \bar{C}_\infty) + \left(\dfrac{\nu}{\bar{K}} + \dfrac{\sigma B_0^2}{\rho}\right)(\bar{U}_\infty - \bar{u}) \end{array} \right\} \tag{8.2.8}$$

Introducing the non-dimensional variables

$$\left\{ \begin{array}{l} \bar{u} = uU_0, \ \ \bar{v} = vV_0, \ \ \bar{U}_\infty = U_\infty U_0, \ \ \bar{u}_p = U_p U_0, \ \ y = \dfrac{V_0 \bar{y}}{\nu}, \\[4mm] \bar{K} = \dfrac{\nu^2 K}{V_0^2}, \ \ \bar{T} = \bar{T}_\infty + \theta(\bar{T}_w - \bar{T}_\infty), \ \ \bar{C} = \bar{C}_\infty + \phi(\bar{C}_w - \bar{C}_\infty), \\[4mm] Gr = \dfrac{\nu g\beta(\bar{T}_w - \bar{T}_\infty)}{U_0 V_0^2}, \ \ Gm = \dfrac{\nu g\bar{\beta}(\bar{C}_w - \bar{C}_\infty)}{U_0 V_0^2}, \ \ M = \dfrac{\sigma B_0^2 \nu}{\rho V_0^2}, \\[4mm] t = \dfrac{\bar{t}V_0^2}{\nu}, \ \ n = \dfrac{\bar{n}\,V_0^2}{\nu}, \ \ Pr = \dfrac{\nu\rho C_p}{\kappa} = \dfrac{\nu}{\alpha}, \\[4mm] F = \dfrac{4\nu\,\bar{I}}{\rho C_p V_0^2}, \ \ Sc = \dfrac{\nu}{D}, \ \ Q = \dfrac{Q_0\nu}{\rho C_p V_0^2}, \ \ C_r = \dfrac{\nu\bar{C}_r}{V_0^2} \end{array} \right\} \tag{8.2.9}$$

On using (8.2.9), the equations (8.2.8), (8.2.2) and (8.2.3) become

$$\frac{\partial u}{\partial t} - (1 + \varepsilon Ae^{nt})\frac{\partial u}{\partial y} = \frac{dU_\infty}{dt} + \frac{\partial^2 u}{\partial y^2} + Gr\theta + Gm\phi + N(U_\infty - u), \tag{8.2.10}$$

$$\frac{\partial \theta}{\partial t} - (1 + \varepsilon Ae^{nt})\frac{\partial \theta}{\partial y} = \frac{1}{Pr}\frac{\partial^2 \theta}{\partial y^2} - F\theta - Q\theta, \tag{8.2.11}$$

$$\frac{\partial \phi}{\partial t} - (1 + \varepsilon Ae^{nt})\frac{\partial \phi}{\partial y} = \frac{1}{Sc}\frac{\partial^2 \phi}{\partial y^2} - C_r\phi, \tag{8.2.12}$$

where $N = M + K^{-1}$, Gr is the thermal Grashoff number, Gm is the solutal Grashoff number, Pr is the Prandtl number, M is the magnetic field parameter, Sc is the Schmidt

number, Q is the dimensionless heat generation /absorption parameter, C_r is the chemical reaction parameter and F is the radiation parameter.

The boundary conditions (8.2.5) reduce to following non-dimensional form

$$\left.\begin{cases} u = u_{slip} = \phi_1 \dfrac{\partial u}{\partial y}, \quad \theta = 1, \quad \phi = 1 \quad at \ y = 0 \\[2mm] u \to U_\infty = 1 + \varepsilon e^{nt}, \quad \theta \to 0, \quad \phi \to 0 \quad as \ y \to \infty \end{cases}\right\}, \tag{8.2.13}$$

where $\phi_1 = \dfrac{\sqrt{K}}{\alpha}$.

8.3 Method of Solution:

The equations (8.2.10)-(8.2.12) represent a set of partial differential equations and thus in order to reduce these into a set of ordinary differential equations in dimensionless form, we assume the following for velocity, temperature and concentration as,

$$\begin{cases} u = u_0(y) + \varepsilon e^{nt} u_1(y) + 0(\varepsilon^2) \\[2mm] \theta = \theta_0(y) + \varepsilon e^{nt} \theta_1(y) + 0(\varepsilon^2) \\[2mm] \phi = \phi_0(y) + \varepsilon e^{nt} \phi_1(y) + 0(\varepsilon^2) \end{cases}, \tag{8.3.1}$$

Where u_0, θ_0 and ϕ_0 are mean velocity, mean temperature and mean concentration respectively.

Substituting the equation (8.3.1) into equations (8.2.10)-(8.2.12), equating the harmonic and non-harmonic terms and neglecting the higher-order terms of $0(\varepsilon^2)$, we obtain the following pairs of equations for $(u_0, \theta_0 \ \phi_0)$ and (u_1, θ_1, ϕ_1).

$$u_0'' + u_0' - Nu_0 = -N - Gr\theta_0 - Gm\phi_0, \tag{8.3.2}$$

$$u_1'' + u_1' - (N + n)u_1 = -(N + n) - Au_0' - Gr\theta_1 - Gm\phi_1, \tag{8.3.3}$$

$$\theta_0'' + Pr\theta_0' - (F + Q)Pr\theta_0 = 0,$$ (8.3.4)

$$\theta_1'' + Pr\theta_1' - Pr(F + Q + n)\theta_1 = -APr\theta_0',$$ (8.3.5)

$$\phi_0'' + Sc\,\phi_0' - C_rSc\,\phi_0 = 0,$$ (8.3.6)

$$\phi_1'' + Sc\,\phi_1' - Sc(C_r + n)\,\phi_1 = -ASc\,\phi_0',$$ (8.3.7)

The corresponding boundary conditions are

$$\begin{cases} \begin{pmatrix} u_0 = \phi_1 u_0', & u_1 = \phi_1 u_1', & \theta_0 = 1, \\ \theta_1 = 0, & \phi_0 = 1, & \phi_1 = 0 \end{pmatrix} & at \ \ y = 0 \\ \begin{pmatrix} u_0 \to 1, & u_1 \to 0, & \theta_0 \to 0, \\ \theta_1 \to 0, & \phi_0 \to 0, & \phi_1 \to 0 \end{pmatrix} & as \ \ y \to \infty \end{cases}$$ (8.3.8)

On using the boundary conditions (8.3.8), the solutions of equations (8.3.2) to (8.3.7) are obtained as follows:

$$\theta_0 = e^{-\xi_2 y},$$ (8.3.9)

$$\theta_1 = E_1 e^{-\xi_2 y} - E_1 e^{-\xi_4 y},$$ (8.3.10)

$$\phi_0 = e^{-\xi_6 y},$$ (8.3.11)

$$\phi_1 = E_2 e^{\xi_6 y} - E_2 e^{\xi_8 y},$$ (8.3.12)

$$u_0 = 1 + C_1 e^{-\xi_{10} y} + C_2 e^{-\xi_6 y} + C_3 e^{-\xi_2 y},$$ (8.3.13)

$$u_1 = \begin{cases} C_4 e^{-\xi_{12} y} + C_5 e^{-\xi_{10} y} + C_6 e^{-\xi_6 y} \\ +C_7 e^{-\xi_2 y} + C_8 e^{-\xi_8 y} + C_9 e^{-\xi_6 y} \end{cases}.$$ (8.3.14)

Thus the expression for the velocity, temperature and concentration profiles are as follows

$$u(y,t) = \begin{cases} 1 + C_1 e^{-\xi_{10}y} + C_2 e^{-\xi_6 y} + C_3 e^{-\xi_2 y} \\ +\varepsilon e^{nt} \begin{pmatrix} C_4 e^{-\xi_{12}y} + C_5 e^{-\xi_{10}y} + C_6 e^{-\xi_6 y} \\ +C_7 e^{-\xi_2 y} + C_8 e^{-\xi_8 y} + C_9 e^{-\xi_6 y} \end{pmatrix} \end{cases}, \qquad (8.3.15)$$

$$\theta(y,t) = \left\{ e^{-\xi_2 y} + \varepsilon e^{nt} \left(E_1 e^{-\xi_2 y} - E_1 e^{-\xi_4 y} \right) \right\}, \qquad (8.3.16)$$

$$\phi(y,t) = \left\{ e^{-\xi_6 y} + \varepsilon e^{nt} \left(E_2 e^{\xi_6 y} - E_2 e^{\xi_8 y} \right) \right\}, \qquad (8.3.17)$$

The skin friction at the wall is given by

$$\tau = \left(\frac{\partial u}{\partial y} \right)_{y=0} = - \begin{cases} (C_1 \xi_{10} + C_2 \xi_6 + C_3 \xi_2) \\ \varepsilon e^{nt} \begin{pmatrix} C_4 \xi_{12} + C_5 \xi_{10} + C_6 \xi_6 \\ +C_7 \xi_2 + C_8 \xi_8 + C_9 \xi_6 \end{pmatrix} \end{cases} \qquad (8.3.18)$$

The rate of heat transfer in terms of Nusselt number is

$$Nu = \left(\frac{\partial \theta}{\partial y} \right)_{y=0} = - \left\{ \xi_2 + \varepsilon e^{nt} (\xi_2 - \xi_4) E_1 \right\} \qquad (8.3.19)$$

The rate of mass transfer in terms of Sherwood number is

$$Sh = - \left\{ \xi_6 + \varepsilon e^{nt} (\xi_6 - \xi_8) E_2 \right\}, \qquad (8.3.20)$$

8.4 Validity:

The present results are found in good agreement with the results of Kartikeyan (2013) in the absence of the *mass transfer* and *chemical reaction parameter*.

Table 8.4(a): Comparison of the flow velocity profiles with Kartikeyan (2013) for different times when $Gr = 6$, $Pr = 0.7$, $K = 1$, $Q = 0.5$, $F = 1$, $M = 3$, $n = 0.1$, $\varepsilon = 0.2$, $A = 1$ and $\emptyset_1 = 0.3$:

Table 8.4(a)						
	Present results			Kartikeyan (2013)		
y	$t=1$	$t=3$	$t=5$	$t=1$	$t=3$	$t=5$
0.0	0.9869016	0.985065	0.9871037	0.9868610	0.985098	0.9871109
0.2	1.4622913	1.520964	1.5870358	1.4622907	1.5209514	1.5870347
0.4	1.2990856	1.3529170	1.4270674	1.2990901	1.3529201	1.4270501
0.6	1.2350955	1.2973815	1.3571093	1.2350937	1.2973753	1.3571207
0.8	1.2280961	1.2879350	1.3280624	1.2280868	1.2879276	1.3280395
1.0	1.2279641	1.2880147	1.3275397	1.2279517	1.2880155	1.3275351

Table 8.4(b): Comparison of the shear stress profiles with Kartikeyan (2013) for different heat generation and radiation when $Gr = 2$, $Pr = 0.7$, $K = 1$, $F = 1$, $M = 2$, $n = 0.1$, $t = 1$, $\varepsilon = 0.2$, $A=1$ and $\emptyset_1=1$:

Table 8.4(b)						
	Present results			Kartikeyan (2013)		
M	$Q=0$	$Q=2$	$Q=4$	$Q=0$	$Q=2$	$Q=4$
0	0.6528597	0.5217811	0.4600972	0.6528762	0.5217709	0.4600972
2	0.4175608	0.3580979	0.3274248	0.4175578	0.3580991	0.3274248
4	0.3305581	0.2931631	0.2729917	0.3305672	0.2931647	0.2729917
6	0.2834952	0.2567361	0.2418808	0.2834967	0.2567318	0.2418808

In Table 8.4 (*a*), it has been seen that the velocity profiles are enhanced by the effect of time parameter. In Table 8.4(b), it is marked that the shear stresses are reduced by the effect of heat generation parameter. From both these Tables it is concluded that the absolute difference between the present and the previous results is very less than unity ($<10^{-5}$) and which validated the flow model for further investigation.

8.5 Results and Discussion:

The numerical calculations have been carried out to discuss physical significance of various parameters involved in the results (8.3.15) to (8.3.20). The effects of the key parameters entering in the governing equations on the velocity, temperature, concentration, skin friction, Nusselt number and Sherwood number are shown through graphs.
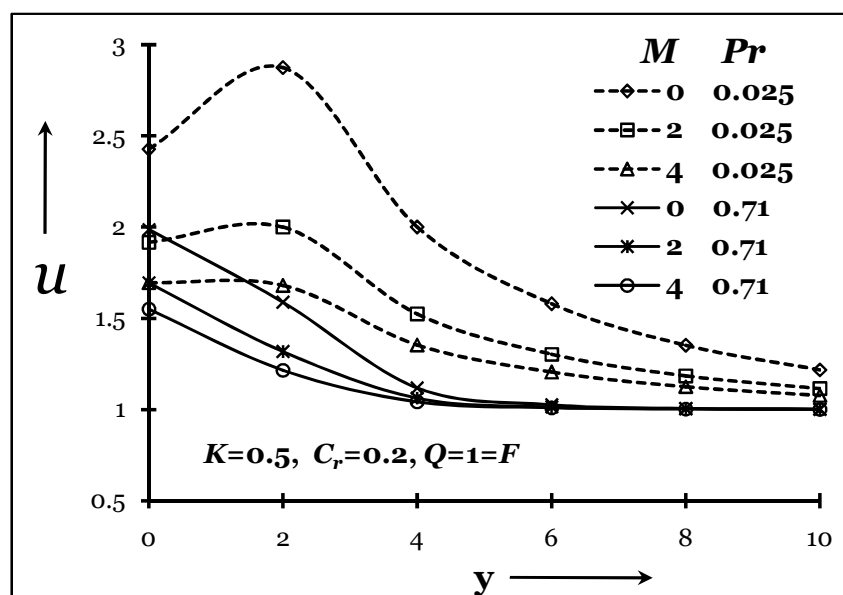

Fig. 8.5 (i): Velocity distribution for *M* and *Pr*

The effect of magnetic parameter M on velocity profiles in the boundary layer is depicted in Fig. 8.5(i) for both the cases of Pr = 0.025 (mercury) and Pr = 0.71 (air) by keeping other parameters of the flow field as constant. From this figure it is seen that the velocity starts from minimum value at the surface and is increased till it attains the peak value and then starts decreasing until the boundary condition matches as $y \to \infty$ for all the values of the magnetic field parameter. It is interesting to note that the effect of magnetic field is to decelerate the velocity of the flow field to an

appreciable amount throughout the boundary layer. The effect of magnetic field is more prominent at the point of the peak value i.e. the peak value drastically decreases with increase in the value of the magnetic field because the presence of magnetic field in an electrically conducting fluid produces a force called the Lorentz force, which acts against the flow on application of the magnetic field in the normal direction. This type of resisting force slows down the fluid velocity as seen clearly in this figure. Smaller Pr fluids have higher thermal conductivities so that heat can diffuse away from the vertical surface faster than for higher Pr fluids (thicker boundary layers).
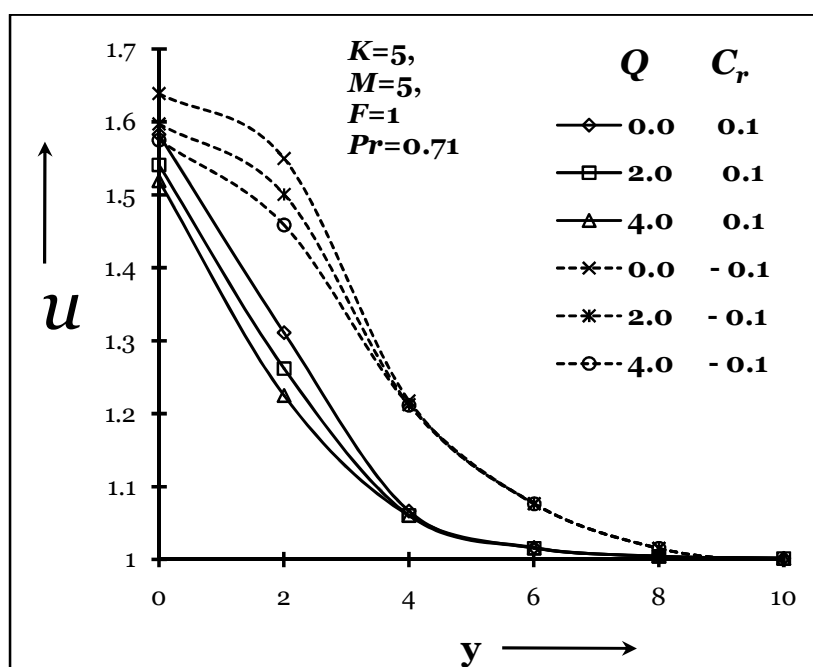
Fig. 8.5 (ii): Velocity distribution for Q and C_r

Fig. 8.5(ii) depicts the variation of dimensionless velocity profiles for different values of heat generation (Q) for both generative ($C_r = 1.0 > 0$) and destructive ($C_r = -1.0 < 0$) chemical reactions. It is observed from this figure that the velocity distribution is decreased at all points of the flow field with increasing in the heat generation. This shows that the destructive chemical reaction have an enhancing effect on the velocity

distribution of the flow field. It is interesting to note that the generative chemical reaction have the tendency in formation of depression velocity profile near the plate.

Fig. 8.5 (iii) illustrates the effect of radiation (F) on the horizontal velocity in the momentum boundary layer with different slip parameters ($\emptyset_1 = 0.3$ and 10). We note from this figure that there is decrease in the horizontal velocity profiles with increase in the radiation parameter F. The increase of the radiation parameter F leads to decrease the boundary layer thickness and to enhance the heat transfer rate in the presence of thermal and solutal buoyancy forces.
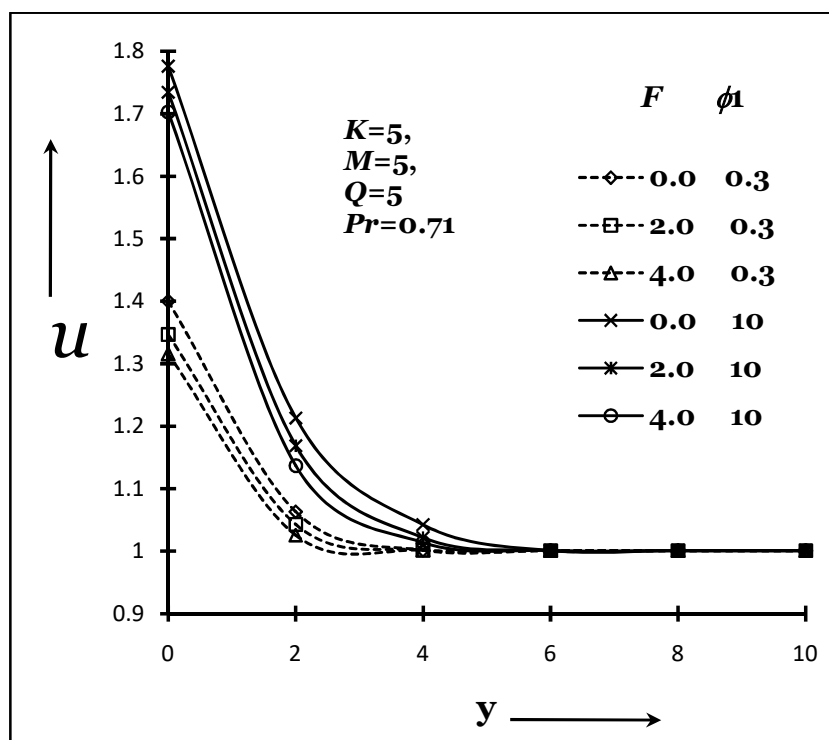
Fig. 8.5 (iii): Velocity distribution for F and ϕ_1

The effect of porosity of the medium on velocity profiles in the boundary layer is depicted in Fig. 8.5(iv) for both the cases $Sc = 0.30$ (Helium) and $Sc = 0.78$

(Ammonia). From this figure it is seen that the velocity starts from minimum value zero at the surface and is increased till it attains the peak value and then starts decreasing until it reaches to the minimum value at the end of the boundary layer for all the values of porosity. It is significant to note that the effect of porosity is to increase the value of the velocity profile throughout the boundary layer. Moreover, the velocity profile decreases with increase in the value of Schmidt number (*Sc*) i.e. the presence of heavier diffusing species has a retarding effect on the velocity of the flow field.
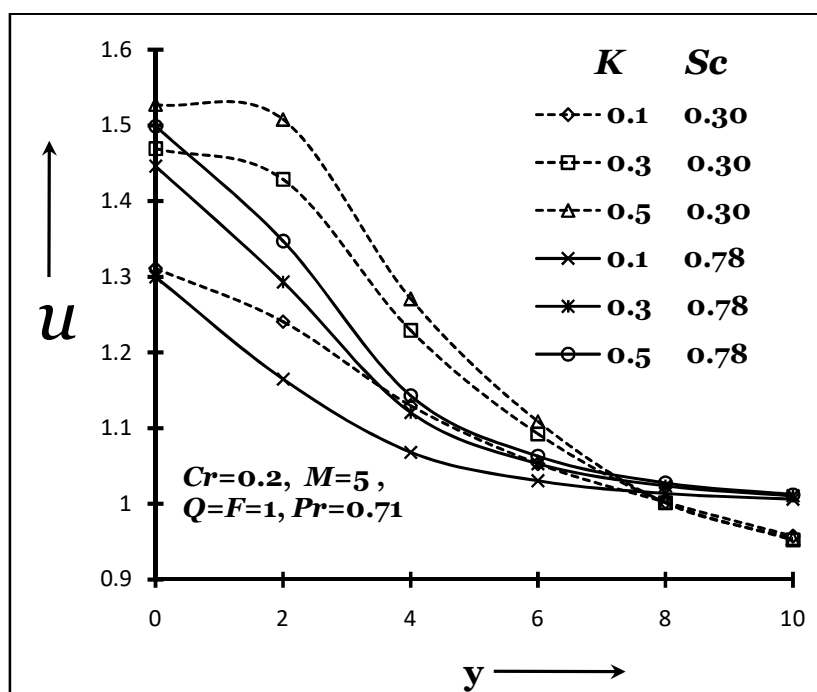

Fig. 8.5 (iv): Velocity distribution for *K* and *Sc*

Fig. 8.5(v) depicts the variation of dimensionless temperature profiles for different values of heat generation (*Q*) rate and thermal radiation (*F*). It has been seen that the temperature profiles are decreased with increasing the heat source parameter *Q* which results in decreasing the thermal boundary layer thickness with stronger heat

generation. Further, it is observed that the temperature is decreased with increasing radiation parameter. This is due to the fact that the decrease in the values of the thermal radiation parameter decreases the flux of energy transport to the fluid and accordingly decreases the fluid temperature in the thermal boundary layer. Thus it is found that the effect of thermal radiation is to reduce heat transfer and due to which there is decrease in the thermal boundary layer thickness.
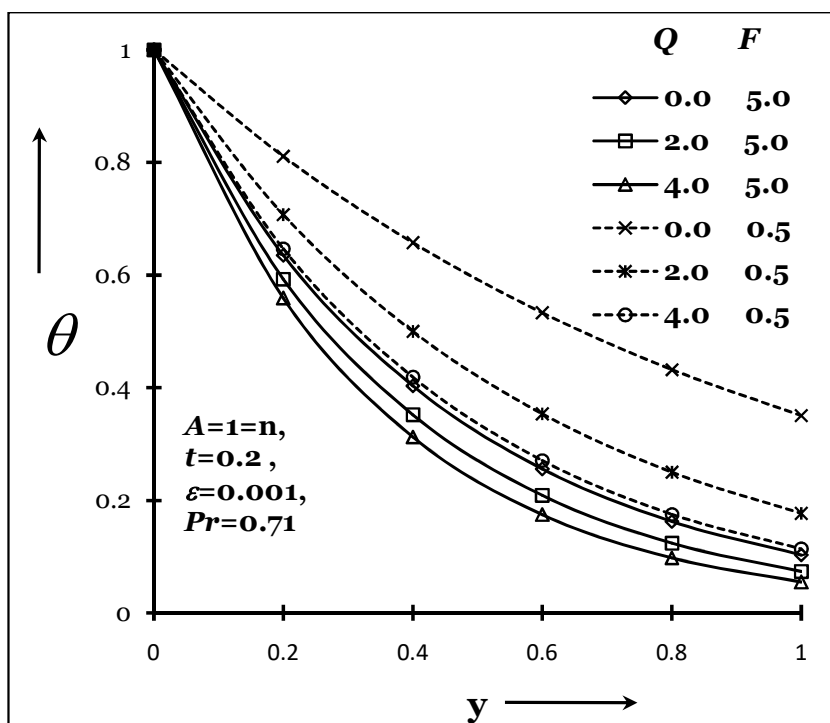

Fig. 8.5 (v): Temperature distribution for *Q* and *F*

The variation of the chemical reaction parameter (C_r) on concentration distribution of the flow field with the diffusion of the foreign mass is shown in Fig. 8.5(vi). The effect of chemical reaction parameter is very crucial in the concentration field; chemical reaction increases the rate of interfacial mass transfer. Generally, whenever the species concentration at the plate surface is higher than the free stream

concentration, a gradual decrease in the concentration profile is observed towards the free stream as in the present case. It is obvious that the influence of increasing the values of C_r decreases the concentration distribution across the solutal boundary layer. The chemical reaction reduces the concentration and hence increases its concentration gradient and its flux. Moreover, concentration distribution is decreased at all the points of the flow field with increase of the Schmidt number (*Sc*) which shows that heavier diffusing species have greater retarding effect on the concentration distribution of the flow field, due to the fact that the boundary layer thickness is greatly decreased with increase in the value of the Schmidt number.
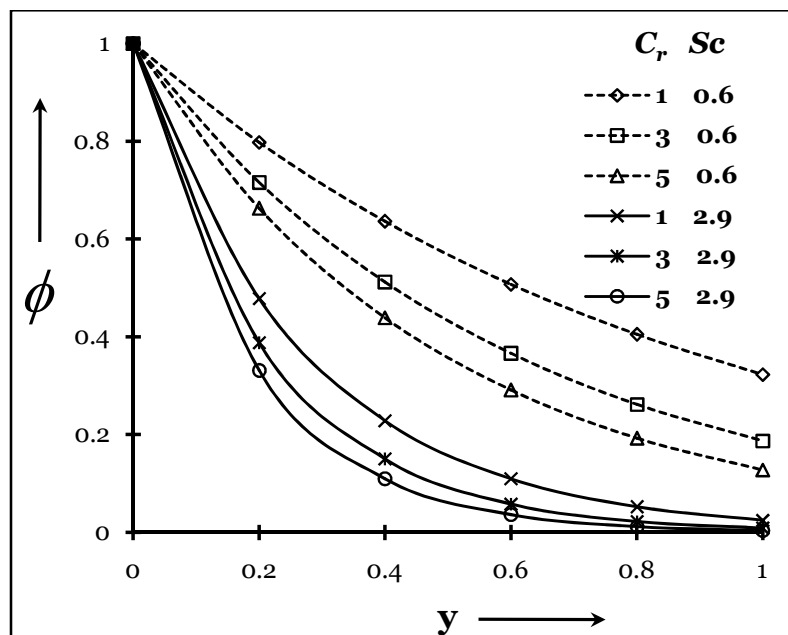

Fig. 8.5 (vi): Concentration distribution for C_r and *Sc*

The velocity gradient at the plate y = 0 in terms of shear stress (τ) with the effects of generative chemical reaction (C_r) and heat generation (Q) is presented in Fig. 8.5 (vii). It is observed that an increase in C_r leads to decrease in the values of velocity gradients. In addition, the curves show the substantial decrease at the plate i.e.

the values of the shear stress fall heavily due to the bigger heat generation. Peak velocity is achieved near the plate which decays to the relevant free stream velocity.
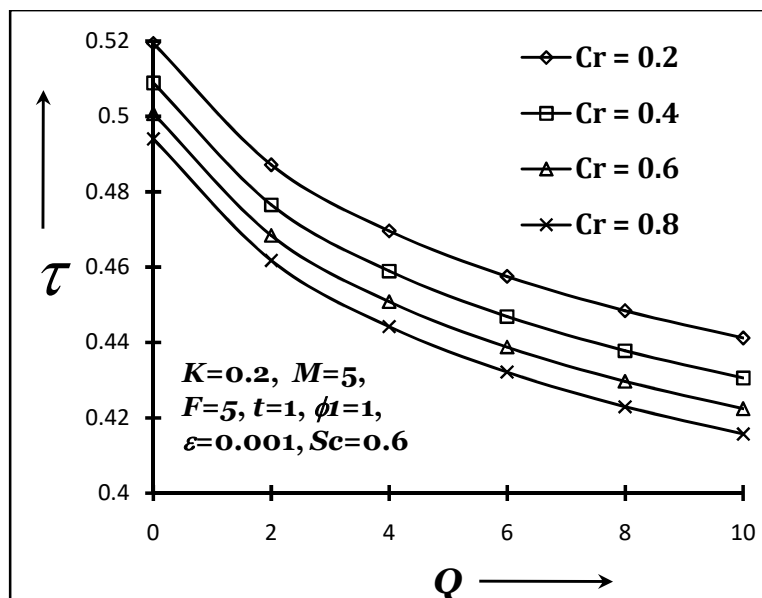
Fig. 8.5 (vii): Shear stress distribution for C_r and Q
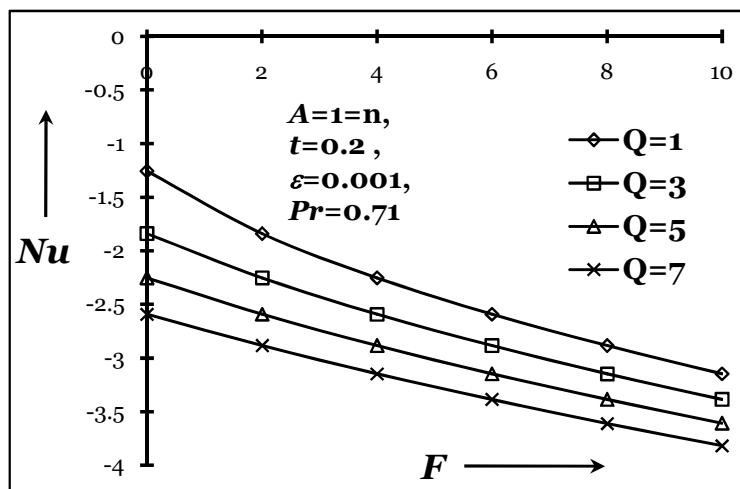
Fig. 8.5 (viii): Nusselt number distribution for F and Q

Fig. 8.5 (viii) illustrates the effects of heat generation (Q) and thermal radiation (R) on the temperature gradient in terms of Nusselt number (Nu). As depicted in this figure, the effect of increasing the value of Q is to increase the value of Nu distribution in the boundary layer. Moreover, Nu is raised by increasing the value of the thermal radiation. All the values of Nu are negative and hence it indicates that the heat is diffused towards the plate y = 0.
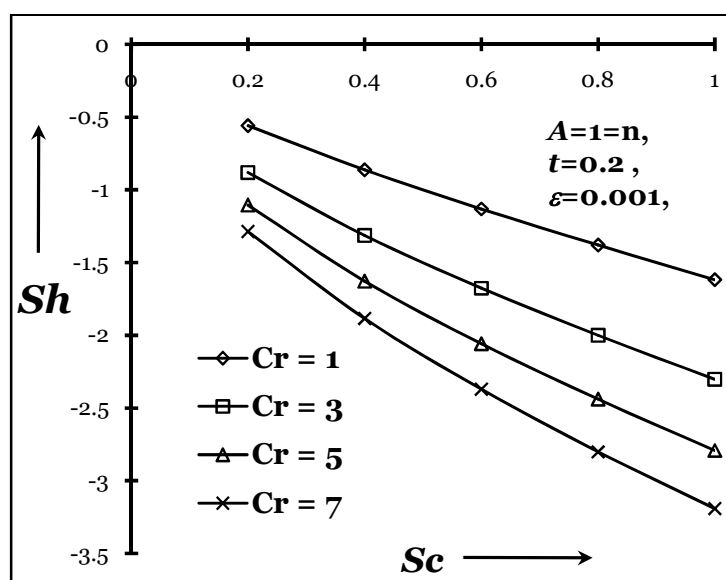

Fig. 8.5 (ix): Sherwood number distribution for C_r and Sc

Fig. 8.5 (ix) shows the effect of Schmidt number (Sc) and chemical reaction (C_r) on concentration gradient at the plate y = 0 in terms of Sherwood number (Sh). It is found that the Sherwood number is increased with increase in Schmidt number and chemical reaction. Moreover, Sh is raised by increasing the value of the Schmidt number (Sc). All the values of Sh are negative and hence it signifies that the mass has diffused towards the plate y = 0.

8.6 Conclusions:

In this problem the influence of chemical reaction on MHD convective flow with heat and mass transfer past a semi-infinite vertical porous plate immersed in a Darcian porous medium in the presence of heat generation and slip flow has been analyzed. The suction velocity normal to the plate and the free stream velocity are considered here periodic functions. The governing system of equations has been solved using perturbation technique. The effects of different key parameters on velocity, temperature, concentration and velocity, temperature, concentration gradients at the plate y = 0 were studied in details. Some important conclusions are given below:

➢ Increasing the heat generation parameter reduces both velocity and temperature.

➢ The velocity is increased with an increase in the permeability of the porous medium parameter.

➢ It is seen that for small values magnetic field the flow velocity is overshoot in presence mercury ($Pr = 0.025$).

➢ An increase in the thermal radiation (F) leads to decrease in the velocity and temperature.

➢ Both the velocity and concentration are reduced with an increase in the Schmidt number (Sc). Moreover, the velocity and concentration are decreased with an increase in the chemical reaction parameter (C_r).

➢ An increase in heat generation/radiation enhances the rate of heat transfer.

➢ An increase in chemical reaction/Schmidt number escalates the rate of mass transfer.

➢ The chemical reaction/ heat generation has a depressing effect on the shear stress (τ).